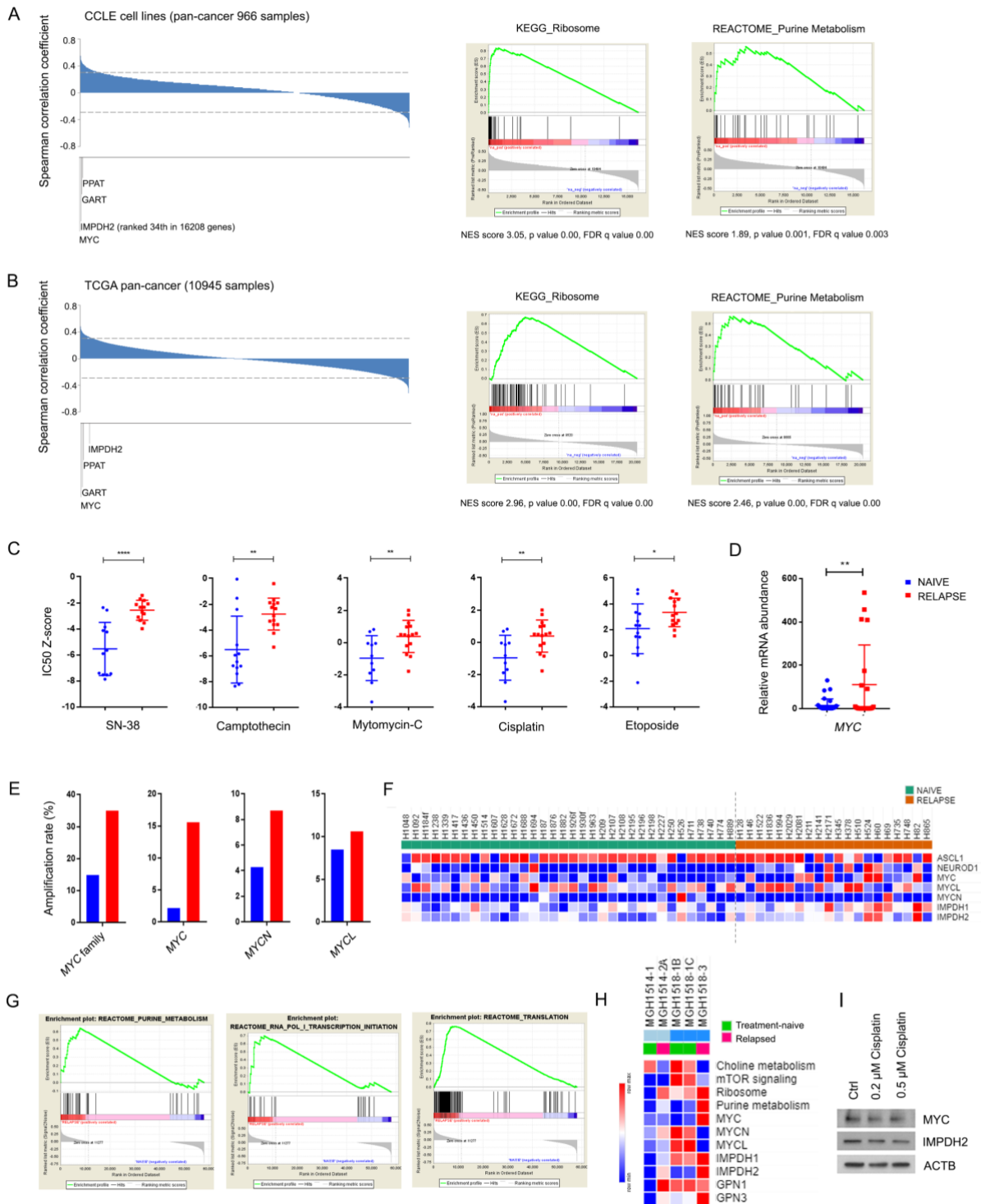


Supplementary Figure 1. Distinct metabolomic subsets of human SCLC tumors. Related to Figure 1.

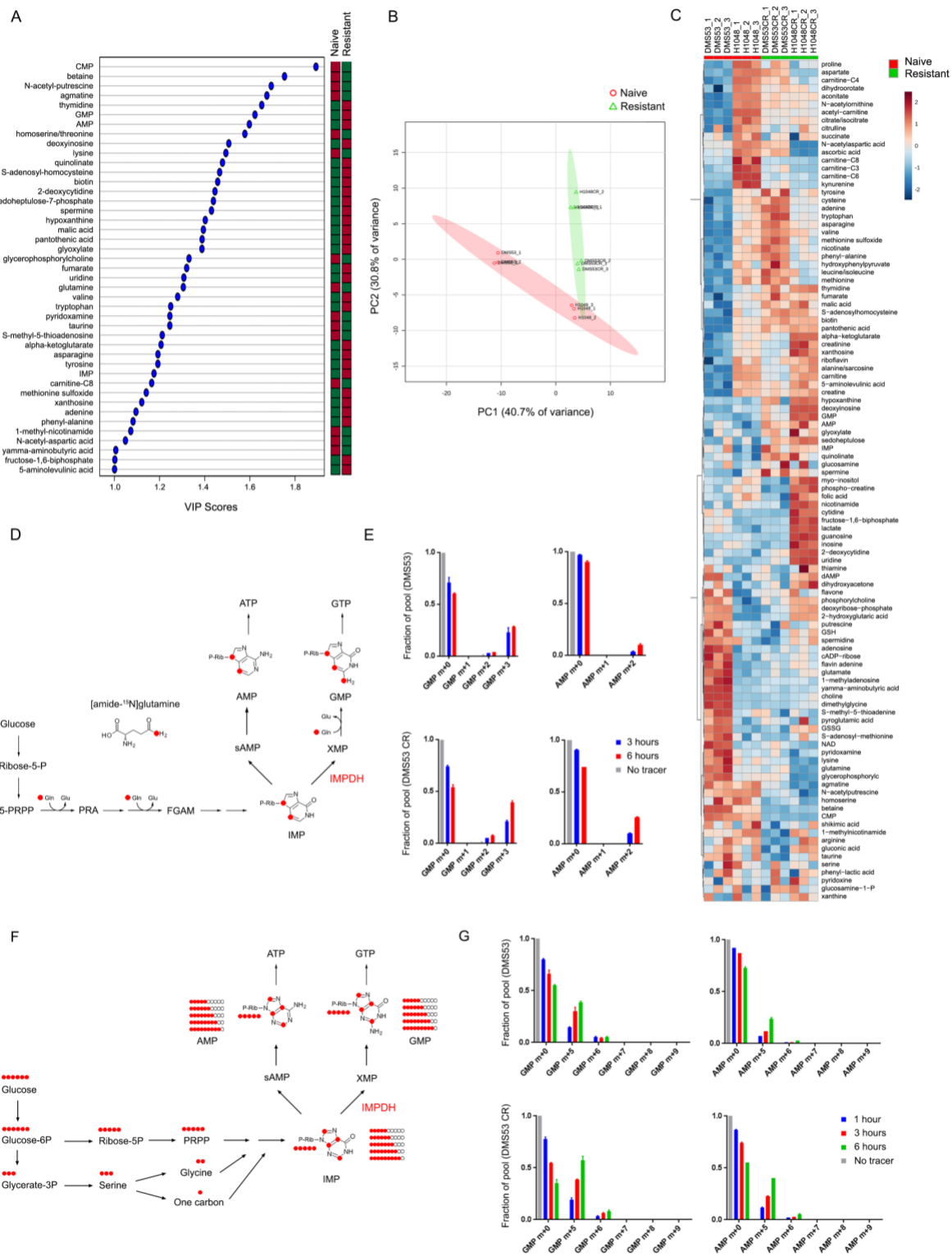
A) Abundance of MYC, MYCN and MYCL in tumors from treatment-naïve SCLC patients. B) Abundance of MYC in select tumors from panel A, with H1436 cells infected with pCW57 empty vector (EV) or pCW57-MYC (MYC), then treated with 1000 ng/ml doxycycline for 72 h to induce MYC, as positive and negative controls for MYC expression. Molecular weight markers are indicated on the left. C) The heatmap shows unsupervised clustering based on the relative abundance of metabolites in primary tumors from 43 treatment-naïve SCLC patients. Peak areas of each metabolite were normalized by total ion count. Data are displayed for three fragments from each tumor. The four molecular classes are color-coded as indicated in the key at the top. Coloring on the heatmap reflects a log₂ scale.



Supplementary Figure 2. Enhanced purine biosynthesis in chemoresistant SCLC. Related to Figure 2.

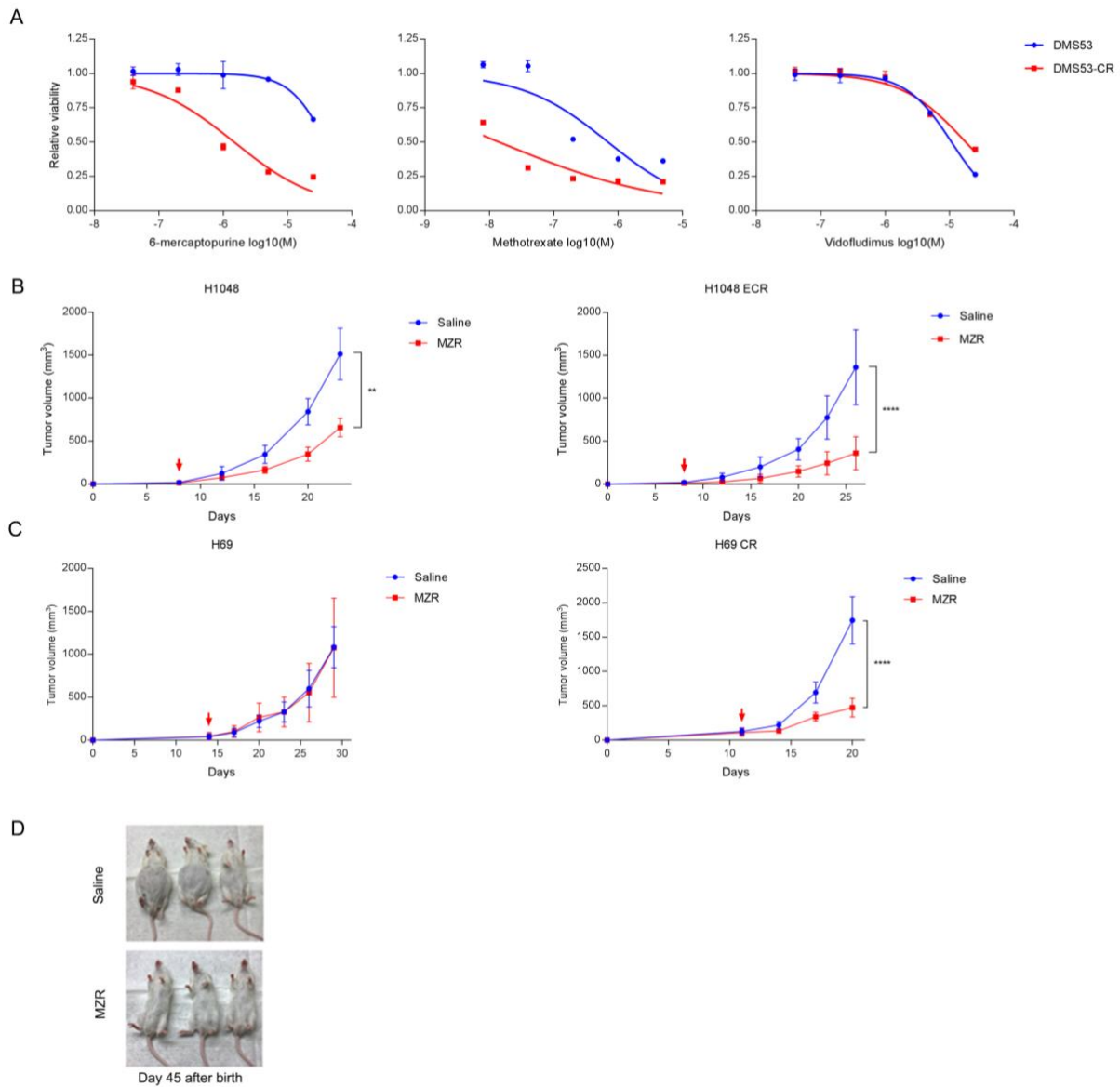
A) *Left*, Spearman's correlation coefficients between *MYC* mRNA abundance and all other transcripts in cells from CCLC. Dashed lines demarcate $p=0.05$. *Right*, Correlation of the "KEGG_Ribosome" and "REACTOME_Purine Metabolism" gene sets with *MYC* mRNA. B) *Left*, Spearman's correlation coefficients between *MYC* mRNA abundance and all other transcripts in human tumors from the pan-cancer TCGA database. Dashed lines demarcate $p=0.05$. *Right*, Correlation of the "KEGG_Ribosome" and "REACTOME_Purine Metabolism" gene sets with *MYC* mRNA. C) IC_{50} of SN-38, camptothecin, mitomycin-C, cisplatin and etoposide in 28 human SCLC cell lines derived from treatment-naïve or relapsed patients from the Genomics of Drug Sensitivity in Cancer database. * $p < 0.05$, ** $p < 0.01$, **** $p < 0.0001$. D) *MYC* abundance in 54 SCLC cell lines derived from treatment-naïve or relapsed patients. ** $p < 0.01$. E) Genome amplification rate of *MYC*, *MYCL*, *MYCN* in the cell lines analyzed in D. F) Heatmap displaying relative abundance of selected mRNAs in the cell lines analyzed in D. G) Gene set enrichment analysis from mRNA abundances between treatment-naïve and relapsed SCLC cell lines analyzed in D. H) Relative mRNA abundance and pathway scores from paired treatment-naïve and relapsed SCLC PDXs. MGH1514-1 arose from circulating tumor cells and MGH1514-2A arose from a subcutaneous nodule biopsy in the same patient after etoposide and

cisplatin chemotherapy. MGH1518-1B and C arose from mediastinal lymph node biopsies in a treatment-naïve patient, while MGH1518-3 arose from a mediastinal lymph node biopsy in the same patient after etoposide and cisplatin chemotherapy. I) Abundance of MYC and IMPDH2 in DMS53 cells treated with 0, 0.2 or 0.5 μ M cisplatin for 1 week. Data are shown as mean and SD (C,D). Statistical significance was assessed using a two-tailed Student's t-test (C,D).



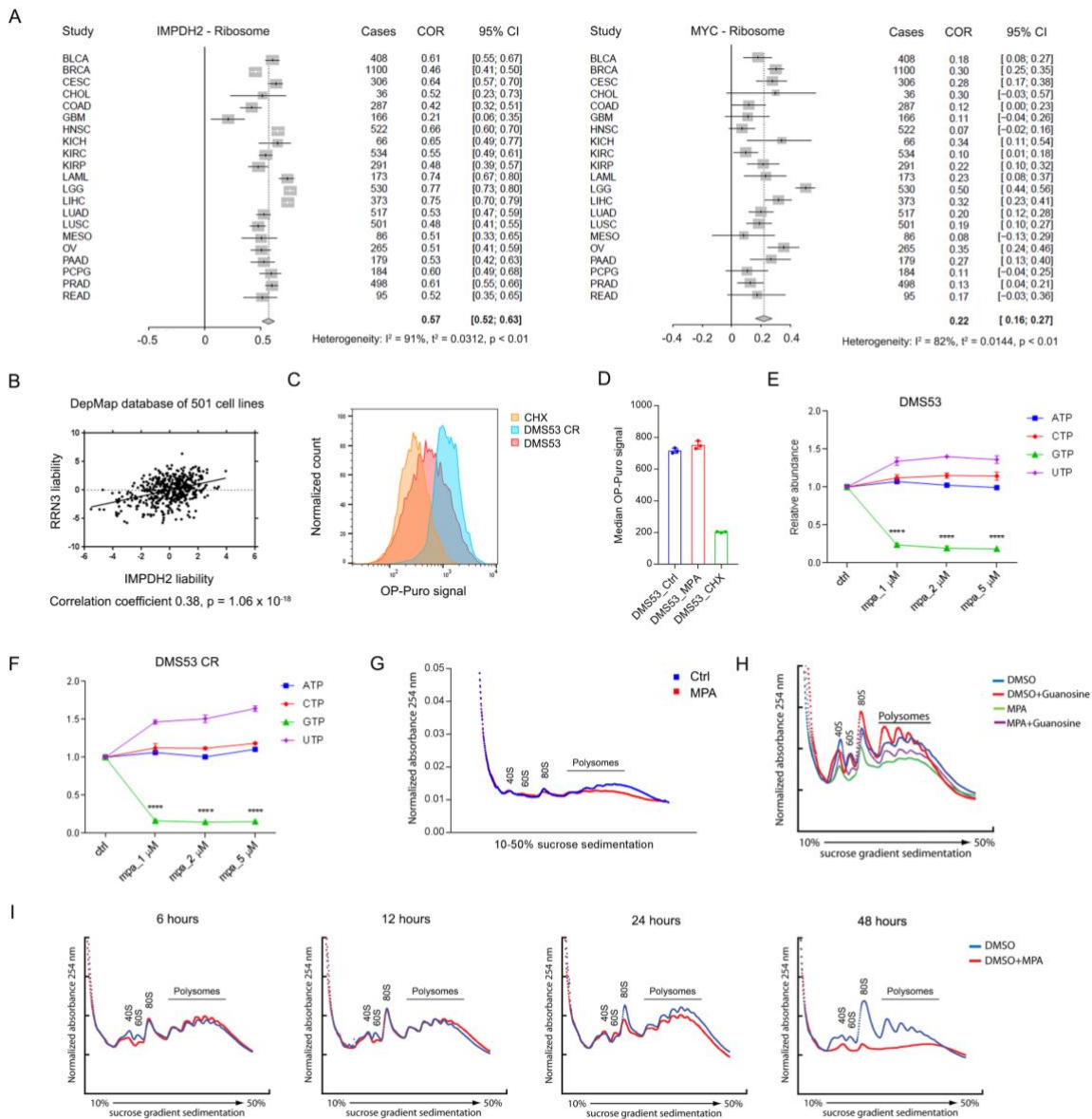
Supplementary Figure 3. Enhanced purine biosynthesis in chemoresistant SCLC. Related to Figure 2.

A) Metabolites discriminating between two isogenic pairs of treatment-naïve and chemoresistant SCLC cell lines subjected to metabolomic analysis. These metabolites have VIP scores of 1.0 or higher. The bar on the right indicates whether each metabolite is more (red) or less (green) abundant in each class. B) Principal component analysis of metabolomic signatures of cells analyzed in A. Individual data points are shown for three independent cultures. C) Heatmap with relative abundance of metabolites analyzed in A. Peak areas of each metabolite were normalized by total ion count. Individual data points are shown for three independent cultures for each cell line. D) Schematic of de novo purine synthesis illustrating labeling from [amide-¹⁵N]glutamine. E) Fractional labeling of GMP and AMP in treatment-naïve and chemoresistant DMS53 cells cultured in medium containing [amide-¹⁵N]glutamine for 3 or 6 h. “No tracer” indicates cells cultured with unlabeled glutamine. F) Schematic of de novo purine synthesis illustrating labeling from [U-¹³C]glucose. G) Fractional labeling of GMP and AMP in treatment-naïve and chemo-resistant DMS53 cells cultured in medium containing [U-¹³C]glucose for 3 or 6 h. “No tracer” indicates cells cultured with unlabeled glucose. Data are shown as mean and SD (E,G).



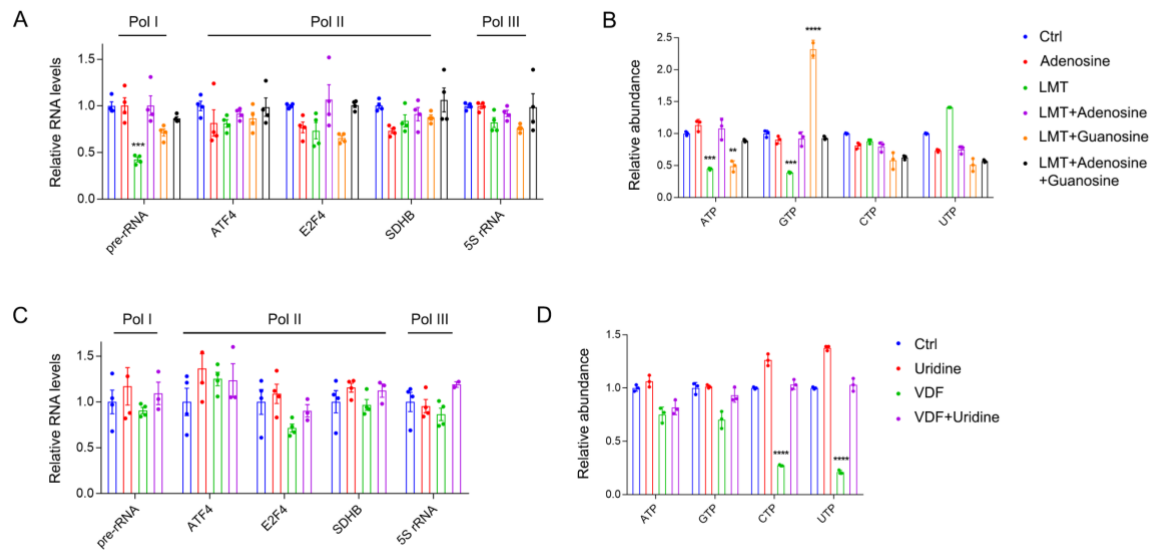
Supplementary Figure 4. IMPDH dependence is a generalizable and actionable metabolic liability in MYC-driven tumors. Related to Figure 3.

A) Drug response curves for DMS53 and DMS53-CR cells to methotrexate, 6-mercaptopurine and vidofludimus. B, C) Growth of subcutaneous xenografts in NSG mice derived from treatment-naïve or chemoresistant H1048 and H69 cells. Mice were treated with saline or mizoribine (100 mg/kg) every other day. The arrow indicates initiation of dosing. Mean and SD for tumor volume were shown for each group (n=5 mice). **p < 0.01, ****p < 0.0001. D) Representative images of *LAP-MYC* mice treated with saline or mizoribine (100 mg/kg) every other day. Photographs were taken on the 45th day of life. Statistical significance was assessed using two-way ANOVA with Tukey's multiple comparisons test (B,C).



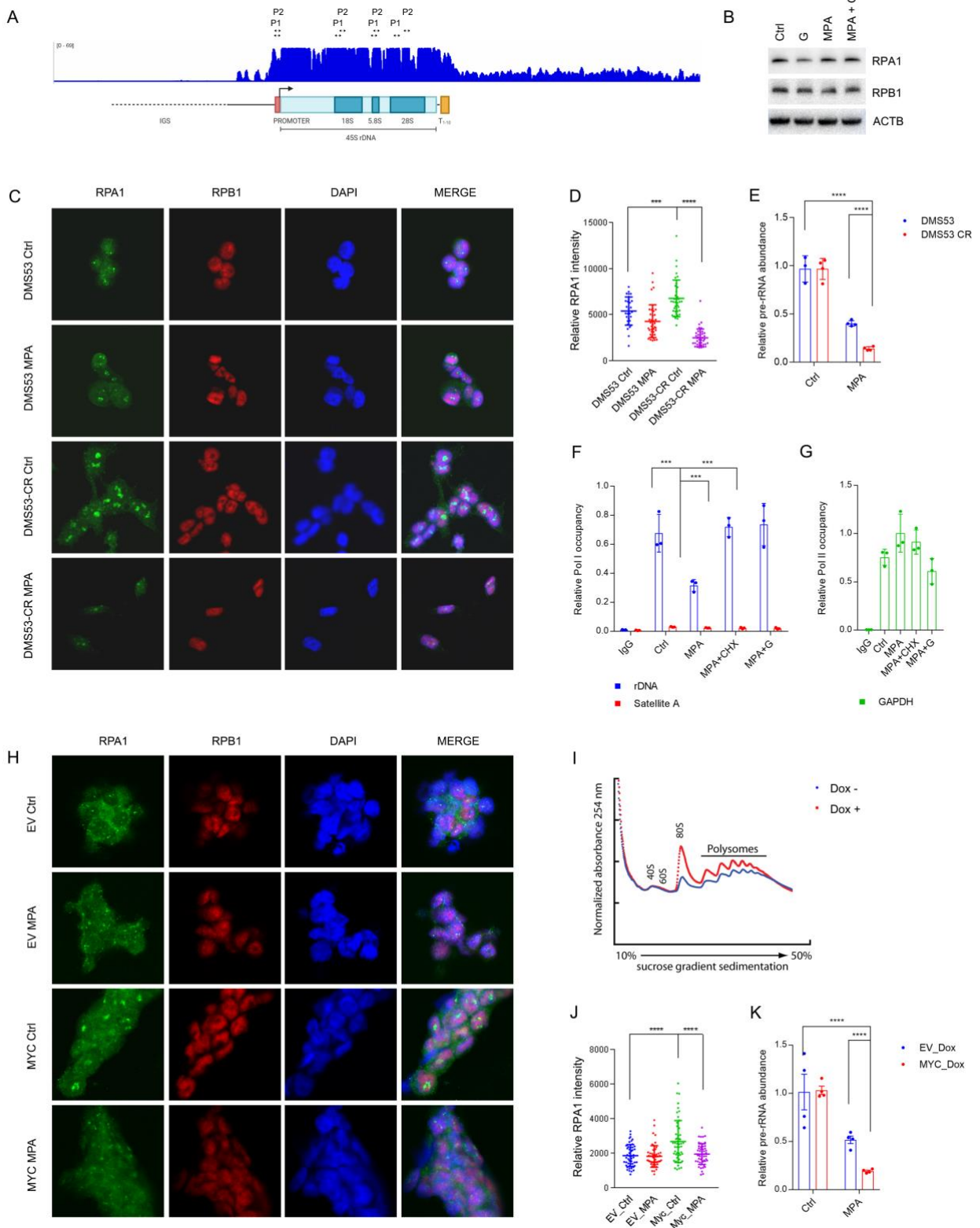
Supplementary Figure 5. Upregulated de novo GTP biosynthesis promotes Pol I activity in chemoresistant SCLC cells. Related to Figure 4.

A) Meta-analysis of correlations between mRNA abundance of ribosomal genes with *MYC* or *IMPDH2* in primary human tumors from the pan-cancer TCGA database. B) Correlation between gene essentiality values for *IMPDH2* and *RRN3* in 501 cell lines from the Achilles Project database. Data are from the DepMap RNAi dataset_20180510, where *RRN3* was top-scoring co-dependent gene with *IMPDH2*. C) Distribution of OP-Puro signal in DMS53 treatment-naïve and chemoresistant (CR) cells. As a positive control for suppressed translation, DMS53-CR cells were treated with 10 $\mu\text{g/ml}$ CHX treatment for 30 min. D) OP-Puro signal in DMS53 cells treated with vehicle or 5 μM MPA for 24 h or 10 $\mu\text{g/ml}$ CHX treatment for 30 min as a positive control for suppressed translation. E, F) Abundance of ATP, CTP, GTP and UTP in DMS53 and DMS53-CR cells treated with 1, 2, or 5 μM MPA or vehicle for 8 h. **** $p < 0.0001$. G) Ribosome abundance in DMS53 cells treated with vehicle or 5 μM MPA for 24 h. H) Ribosome abundance in H82 cells treated with vehicle or 5 μM MPA, with or without 10 μM guanosine for 48 h. I) Ribosome abundance in H82 cells treated with vehicle or 5 μM MPA for 6, 12, 24 or 48 h.



Supplementary Figure 6. Upregulated de novo GTP biosynthesis promotes Pol I activity in chemoresistant SCLC cells. Related to Figure 4.

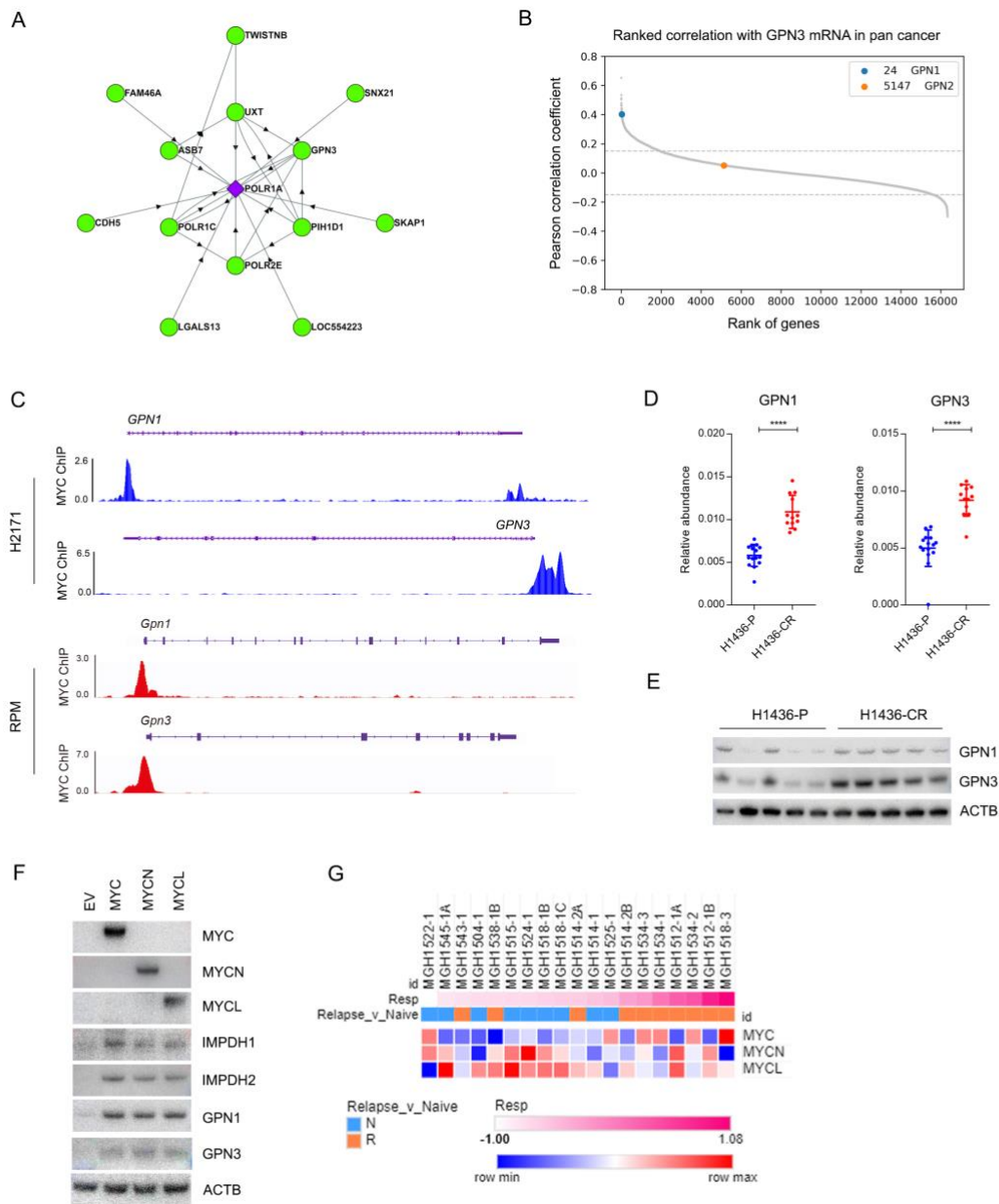
A) Abundance of Pol I, II or III transcripts in DMS53-CR cells treated with vehicle or 25 μ M lometrexol (LMT), with or without 50 μ M adenosine and/or guanosine for 8 h. *** p < 0.001. B) ATP, GTP, CTP and UTP levels in cells from A. ** p < 0.01, *** p < 0.001, **** p < 0.0001. C) Abundance of Pol I, II or III transcripts in DMS53-CR treated with vehicle or 10 μ M vidofludimus (VDF), with or without 50 μ M uridine for 8 h. D) ATP, GTP, CTP and UTP levels in cells from C. **** p < 0.0001. Data are shown as mean and SD (B,D), mean and SEM (A,C). Statistical significance was assessed using one-way ANOVA with Tukey's multiple comparisons test (A-D).



Supplementary Figure 7. Pol I localization to the ribosomal DNA is sensitive to GTP abundance. Related to Figure 5.

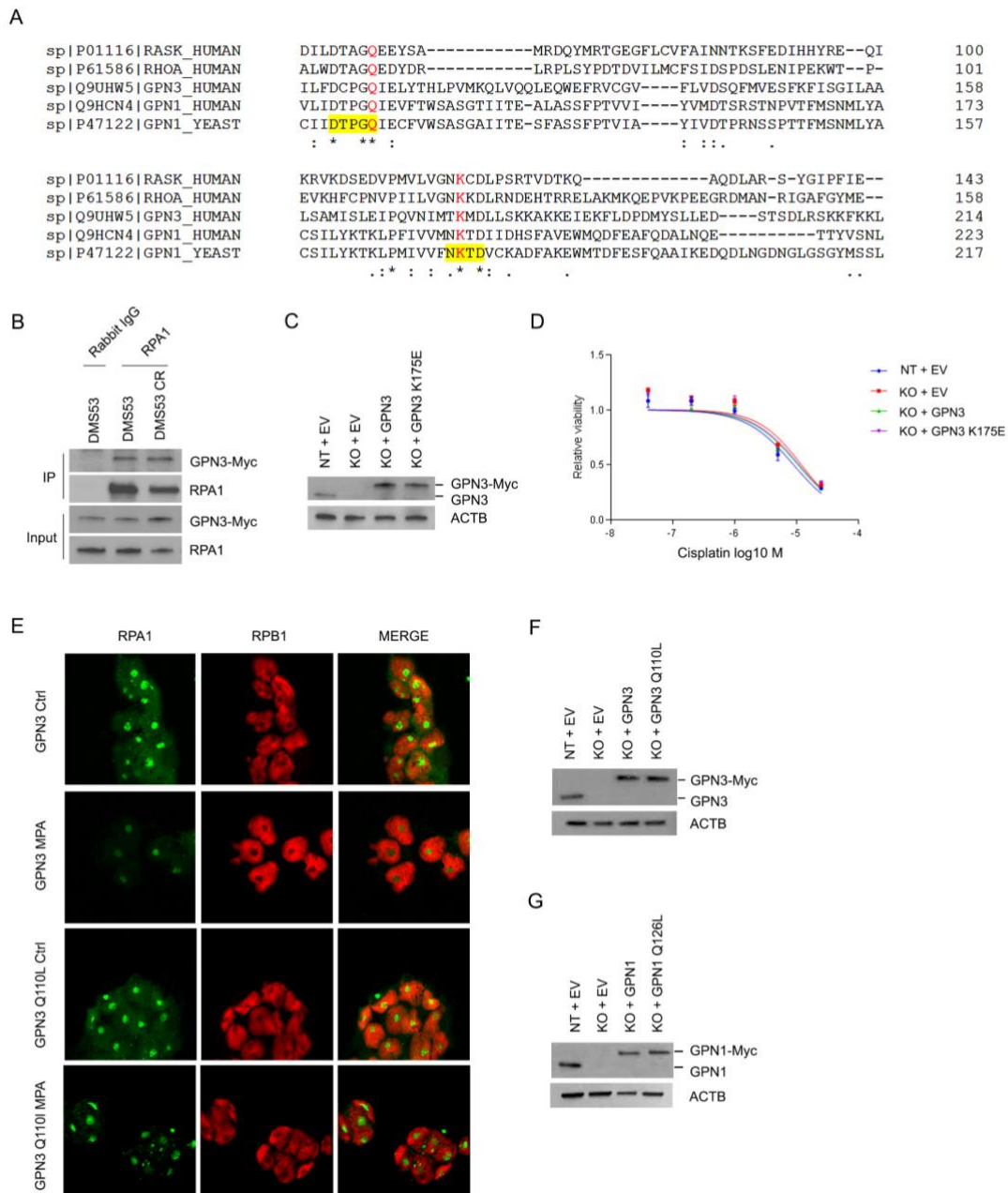
A) RPA1 binding to rDNA in human mammary epithelial cells. B) Abundance of RPA1 and RPB1 in DMS53-CR cells treated with MPA or vehicle, with or without guanosine for 12 h. C) Localization of RPA1 and RPB1 in DMS53 and DMS53-CR cells treated with 1 μ M MPA or vehicle for 12 h. Nuclei are stained with DAPI. Original magnification, 63x. D) Nuclear RPA1 immunofluorescence signals in cells from C. *** $p < 0.001$, **** $p < 0.0001$. E) Abundance of pre-rRNA in DMS53 and DMS53-CR cells treated with 1 μ M MPA or vehicle for 8 h. **** $p < 0.0001$. F) qPCR for rDNA promoter and Satellite A sequences after ChIP with an anti-RPA1 antibody or rabbit IgG control in H82 cells treated with vehicle or 1 μ M MPA, with or without 20 μ M guanosine, 1 μ M cycloheximide for 6 h. *** $p < 0.001$. G) qPCR for *GAPDH* promoter sequences after ChIP with an anti-RPB1 antibody or rabbit IgG control in cells from F. H) Localization of RPA1 and RPB1 in H1436 cells expressing doxycycline-inducible empty vector (EV) or MYC induced with 1 μ g/ml doxycycline for 6 days, then treated with 1 μ M MPA or vehicle for 12 h. Nuclei are stained with DAPI. Original magnification, 63x. I) Ribosome abundance in H1436 cells with or without doxycycline-induced

MYC expression. J) Nuclear RPA1 immunofluorescence in H1436 cells expressing empty vector (EV) or MYC induced by doxycycline for 6 days, then treated with 1 μ M MPA or vehicle for 12 h. ****p < 0.0001. K) pre-rRNA abundance in cells from E. ****p < 0.0001. Data are shown as mean and SD (D-G,J,K). Statistical significance was assessed using one-way ANOVA with Tukey's multiple comparisons test (D-G,J,K).



Supplementary Figure 8. GTP abundance regulates Pol I function in Myc^{High} cells in part through GPN1 and GPN3. Related to Figure 6.

A) Interaction network of RPA1 from the BioPlex 2.0 database. *POLR1A* is the gene encoding RPA1. B) Ranked correlation coefficients between *GPN3* mRNA and all other protein-coding genes in 9,879 samples from the pan-cancer TCGA database. Dashed lines demarcate $p < 0.0001$. *GPN1* and another family member, *GPN2*, are shown. C) Chromatin signatures displaying MYC binding at the *GPN1* and *GPN3* loci in MYC^{High} H2171 cells and at the *Gpn1* and *Gpn3* loci in autochthonous SCLCs from RPM mice. D) *GPN1* and *GPN3* mRNA abundance analyzed by quantitative RT-PCR in H1436 parental or chemoresistant tumors induced by 4 cycles of etoposide and cisplatin. Individual data points are shown with mean and SD for 3 replicates of 4 independent tumors from each group. **** $p < 0.0001$. E) *GPN1* and *GPN3* protein abundance in H1436 parental or chemoresistant tumors induced by 4 cycles of etoposide and cisplatin. Protein lysates from 5 independent tumors in each group are shown. F) Protein abundance of MYC, MYCN, MYCL, IMPDH1, IMPDH2, GPN1, GPN3 in H1436 cells infected with pCW57 empty vector (EV) or pCW57 with MYC (MYC), MYCN (MYCN), MYCL-FLAG (MYCL), treated with or without 1000 ng/ml doxycycline for 72 h. G) Relative mRNA abundance of MYC, MYCN, MYCL in treatment-naïve and relapsed SCLC PDXs. Statistical significance was assessed using a two-tailed Student's t-test (D).



Supplementary Figure 9. GTP abundance regulates Pol I function in Myc^{High} cells in part through GPN1 and GPN3. Related to Figure 7,8.

A) Multiple sequence alignment by CLUSTAL Omega of human RASK, RHOA, GPN3, GPN1 and yeast GPN1. Conserved residues corresponding to GPN3 Q110 and K175 are in red and regions of yeast GPN1 involved in GTPase activity (residues 106-110) and GTP binding (residues 173-176) are highlighted in yellow. B) Immunoprecipitation with anti-RPA1 or rabbit IgG followed by western blot for RPA1 and GPN3-Myc in DMS53 and DMS53-CR cells transiently expressing wildtype GPN3-Myc. C) Abundance of native and Myc-tagged GPN3 in DMS53-CR cells subjected to CRISPR/Cas9 genome editing using a non-targeting (NT) gRNA or a gRNA against GPN3 (KO). These cells were then reconstituted with an empty vector (EV) or vectors expressing wild type or K175E-mutant GPN3. D) Cisplatin response curves for cells from C. E) Sample images of RPA1 and RPB1 localization in H82 cells with CRISPR/Cas9-mediated GPN3 knockout and re-expression of wild type or mutant GPN3, treated with 1 μ M MPA or vehicle for 12 h. *** $p < 0.001$. Original magnification, 63x. F) Abundance of native and Myc-tagged GPN3 in H82 cells subjected to CRISPR/Cas9 genome editing using a non-targeting (NT) gRNA or a gRNA against GPN3 (KO). These cells were then reconstituted with an empty vector (EV) or vectors expressing wild type or Q110L-mutant GPN3. G) Abundance of native and Myc-tagged GPN1 in H82 cells subjected to CRISPR/Cas9 genome editing using a non-targeting (NT) gRNA or a gRNA against GPN1 (KO). These cells were then reconstituted with an empty vector (EV) or vectors expressing wild type or Q126L-mutant GPN1.

Supplementary Table 1. Oligonucleotide Sequences.

Name	Sequences (5'-3')
qPCR_pre-rRNA_fwd	GCTCTACCTTACCTACCTGG
qPCR_pre-rRNA_rev	TGAGCCATTCGCAGTTTCAC
qPCR_ATF4_fwd	ATGACCGAAATGAGCTTCCTG
qPCR_ATF4_rev	GCTGGAGAACCCATGAGGT
qPCR_E2F4_fwd	CACCACCAAGTTCGTGTCCC
qPCR_E2F4_rev	GCGTACAGCTAGGGTGTCA
qPCR_SDHB_fwd	ACAGCTCCCCGTATCAAGAAA
qPCR_SDHB_rev	GCATGATCTTCGGAAGGTCAA
qPCR_5S rRNA_fwd	GGCCATACCACCCTGAACGC
qPCR_5S rRNA_rev	CAGCACCCGGTATTCCCAGG
rDNA-ChIP-18s_fwd1	CGCTCTACCTTACCTACCTGGTTG
rDNA-ChIP-18s_rev1	CCCGTCGGCATGTATTAGCTCTAG
rDNA-ChIP-18s_fwd2	AACGTCTGCCCTATCAACTTTCG
rDNA-ChIP-18s_rev2	CTCATTCCAATTACAGGGCCTCG
rDNA-ChIP-5.8s_fwd1	CGACTCTTAGCGGTGGATCACTC
rDNA-ChIP-5.8s_rev1	CCGCAAGTGCGTTCGAAGTGT
rDNA-ChIP-5.8s_fwd2	CGTCGATGAAGAACGCAGCTAG
rDNA-ChIP-5.8s_rev2	AAGCGACGCTCAGACAGGCG
rDNA-ChIP-28s_fwd1	CCCAAAGCGGGTGGTAAACTC
rDNA-ChIP-28s_rev1	CTCTTAACGGTTTTACGCCCTC
rDNA-ChIP-28s_fwd2	AGAGGAAACTCTGGTGGAGGTC
rDNA-ChIP-28s_rev2	TGAGGGAAACTTCGGAGGGAAC
rDNA-ChIP-Promoter_fwd2	AGGTATATCTTTCGCTCCGAGTC
rDNA-ChIP-Promoter_rev2	AGGACAGCGTGTCTAGCAATAAC
rDNA-ChIP-Promoter_fwd1-pos	ATGGTGGCGTTTTTGGGG
rDNA-ChIP-Promoter_rev1-pos	AGGCGGCTCAAGGCAGGAG

Supplementary Table 2. Antibodies.

Reagent	Source	Identifier
Rabbit monoclonal anti-RPL11	Cell Signaling	18163
Mouse monoclonal anti-ASCL1	BD Bioscience	556604
Rabbit polyclonal anti-GPN3	Sigma	HPA047793
Rabbit polyclonal anti-MYCL	Thermo Fisher	PA5-109998
Rabbit polyclonal anti-GPN1	Thermo Fisher	PA557821
Mouse monoclonal anti- β -Actin-peroxidase	Sigma	A3854
Rabbit polyclonal anti-ADSL	Thermo Fisher	PA5-29964
Mouse polyclonal anti-IMPDH1	Sigma	SAB1406036
Rabbit monoclonal anti-IMPDH2	Abcam	ab131158
Rabbit polyclonal anti-MYC	Cell Signaling Technology	9402
Rabbit polyclonal anti-MYCN	Cell Signaling Technology	94055
Rabbit polyclonal anti-RRN3	Abcam	ab112052
Rabbit polyclonal anti-GMPS	Cell Signaling	14602
Rabbit monoclonal anti-RPA1	Cell Signaling Technology	24799
Mouse monoclonal anti-RPB1	Cell Signaling Technology	2629
Rabbit monoclonal anti-RPA1	Cell Signaling Technology	24799
Rabbit polyclonal anti-RPA1	Abcam	ab222065
Rabbit polyclonal anti-RPA1	Abcam	ab241950
Mouse monoclonal anti-Myc-Tag	Cell Signaling Technology	2276
Rabbit polyclonal anti-Ras	Cell Signaling Technology	3965